

Cohesive Clays for Construction and Stabilization of Unpaved Roads

Hamid Mumin, Ph.D., P.Eng., P.Geo.
Professor and Chair
Department of Geology, Brandon University

Riley Cram
M.Sc. Candidate
Department of Geology, Brandon University

Ayat Baig, M.Sc.
Director
Brandon University Micro Analytical Facility

Gideon Jungen
B.Sc. Honours, Brandon University

Zach Toews
B.Sc. Honours, Brandon University

Paper prepared for presentation at the
Green Technologies in Geotechnical and Materials Engineering Session

2020 TAC Conference “The Journey to Safer Roads”

Acknowledgements

We are grateful to the following organizations and people for supporting this investigation over the past 6 years through financial and in-kind support of the research, research equipment and infrastructure, and student salaries. NSERC-IRAP, Mitacs, NSERC Experience Grants, CFI-MFI, City of Brandon, Manitoba Infrastructure, Western Economic Diversification, the City of Brandon and Brandon University. We thank all past students and research partners and colleagues who helped us along the way. We are particularly grateful to Cypher Environmental who have supported us generously from the beginning and provided continuous advice, support and encouragement for the research. We are also very grateful to the Rural Municipality of Cornwallis, who have been tremendous partners and allies in our research, and without whose partnership and willingness to take a chance on new technologies, this work could not have taken place.

Introduction

Unpaved gravel and dirt roads comprise the majority of the transportation network in most parts of Canada. In Saskatchewan and Manitoba alone, they comprise ~270,000 km of the total road network of ~320,000 km (Transportation Canada, 2008). These unpaved roads present a chronic environmental and safety problem, and are a severe financial challenge and burden for most municipalities and governments that maintain them. Better solutions to their construction and maintenance are needed, along with a new dialogue and way of thinking about road infrastructure that is compatible with modern expectations for a sustainable and healthy future.

In this paper, we present a cost effective solution that utilizes local cohesive clay-rich materials, simple technology and basic construction equipment. Roads constructed in this manner are very durable and eliminate the worst environmental problems including most dust and toxic chemicals, and dramatically reduce the amount of aggregate used. There are also major improvements to safety provided by a strong and durable wearing surface with virtual elimination of potholing, rutting, wash boarding and loose aggregate that leads to reduced traction.

The current investigation has taken place in southwestern Manitoba over the past 6 years. The first test roads using the cohesive clay stabilization process were constructed in 2015 in the Rural Municipality (RM) of Cornwallis, which surrounds the east, south and west sides of Brandon, MB (Figure 1). They comprise 3 high traffic municipal roads servicing rural businesses and residents (3.2 km), and one haulage road (Curries Landing Road, 1.6 km) that services ~10 active gravel quarries with ~200 to 250 loaded gravel trucks daily as well as local residents. In 2017, the haulage road was extended an additional 3.2 km to connect to the Trans Canada Highway, and by 2019 the network of clay stabilized roads in the RM of Cornwallis and neighboring municipalities was ~ 15 km (Figure 2). Laboratory investigations including materials characterization, geotechnical properties, strength and durability are carried out at Brandon University in the Laboratory for Applied Research in Resource Geology, the Brandon University Micro-Analytical Facility, and in the Geology Core and Geotechnical Laboratory.

The purpose of this paper is two fold: 1) to familiarize readers with the cohesive clay road stabilization process, and 2) to investigate the variability and characteristics of clay deposits from southwestern Manitoba and determine their suitability for construction of clay stabilized roads. In this investigation, the term “clay” refers to true mineralogical clay species such as montmorillonite or illite etc., and has no particle size inference. The term “clay deposit” refers to any apparently clay-rich soil, till or fluvial deposit that is thought to contain a significant portion of true clay minerals. Clay deposits are not always what they appear to be.

Clay Minerals

Clay minerals and their unique properties of very small micron to submicron grain size, unbalanced stoichiometry (unbalanced electronic charge), and great compositional variation make them very difficult to analyze and characterize. However, it is these same properties that make clay fundamentally critical to the road stabilization process described below and allow them to be used as strong bonding agents that are effective at binding loose aggregate into a semi-solid material of high bearing strength. The pertinent properties of clay are reviewed so readers can appreciate how and why the bonding process functions.

All minerals must have electronically balanced stoichiometry where total cationic charge is balanced by total anionic charge (Klein and Dutrow, 2007). Clays are the only minerals that characteristically defy this fundamental rule. They are formed by the breakdown of other minerals like feldspar, micas and amphiboles in reaction with water. This enables unbalanced structures to form, where for example Al^{3+} substitutes for Si^{4+} , and Fe^{2+} , Mg^{2+} , Mn^{2+} , et al. substitute for Al^{3+} in tetrahedral and octahedral sites, respectively, within the mineral structure (Figure 3). This is referred to as a substitution although it actually takes place during original mineral growth whereby an Al^{3+} occupies a site that normally prefers a cation with a 4^+ charge such as Si^{4+} , and the same occurs with 2^+ cations occupying structural sites that normally require a 3^+ cation like Al^{3+} . The result is a build up of excess negative charge that is compensated and balanced during mineral growth by an overall positive field charge. This positive field charge is created by the presence of water (a polar molecule) and cationic complexes in solution (Sogami and Ise, 1984; Güven, 1992; Mitchell and Soga, 2005). Hence, clays can form with and retain excess negative charge that is distributed about the surface of platy clay mineral particles. Subsequently, these reactive (negatively charged) clays attract and must bond with +ve charged substances such as the hydrogen protons of polar water molecules or any cations or cationic complexes available until overall electronic neutrality is achieved. The excess negative charge gives clays their great capacity to adsorb and hold water, which imparts a plastic behavior to clay-rich materials.

The potential bonding energy of clays is simply the electrostatic attractions between -ve clay surfaces and any +ve charged substance, and is proportional to the amount of excess -ve charge. The ability to adsorb and bond with +ve substances is also responsible for the cation exchange capacity of a clay (CEC) (Holtz et al, 2011; Barnes, 2016). Species with high CEC are referred to as cohesive or swelling clays. They have the greatest excess negative charges, and have the greatest capacity to adsorb water. As water increasingly dominates the interlayer bonding between clay particles, the material swells, loses its strength and becomes plastic. Consequently, soils with a high proportion of swelling clays like smectite (montmorillonite) and vermiculite are generally among the worst of construction materials.

However, clays with the greatest charge imbalance and greatest tendency to adsorb water and lose strength, are the same materials that are best suited to road stabilization and the construction of strongly bonded road surfaces using the technology discussed in this paper. This counter-intuitive process occurs when cations and cationic complexes replace water and dominate the inter-grain bonding between clay mineral surfaces. With inter-grain cation bonding, the material becomes increasingly rigid as clay particles are drawn closer together and the strength of the electrostatic attraction (bond) between clay surfaces and cations increases significantly (Figure 4). Taken to the extreme where most of the water is removed, groups of bonded clay particles may begin to resemble micas (Mitchel and Soga, 2005; Klein and Dutrow, 2007), and the process is somewhat like a synthetic precursor to diagenesis (the conversion of sediment to rock).

The potential strength of electrostatic bonding holding clay mineral particles together is determined by the amount of excess -ve charge and the extent to which water can be removed, leaving behind only cationic polymers. In clay-rich materials, cations are already present in solution between clay particles, in what is often referred to as the diffuse double layer (Mitchel and Soga, 2005). Consequently, removal of water with or without an additional input of cations or cationic polymers may render the clay particles tightly bonded by intervening cations (Figure 4). This bonding potential is harnessed when appropriate construction protocols, materials and catalysts are applied. The type and amount of

cohesive (reactive/charged) clay present in the road material directly impacts the potential strength and durability of the wearing surface of a road as described below.

Road Construction and Stabilization

All normal best practice procedures for road construction apply (e.g. Thompson et al., 2019). Here we are concerned primarily with construction of a stabilized wearing surface, which can be added to an existing road or can be incorporated into the design of a new road. In the present research, this comprises a clay-rich aggregate layer compacted to a thickness of 15 cm to 20 cm, or as thick as needed to serve the intended purpose. To achieve maximum stabilization and durability with excellent functionality, all of the following must be considered: 1) best practices for road preparation and construction, 2) use of appropriate materials and catalyst according to design specifications, 3) testing and monitoring of materials and the construction process, and 4) proper construction protocol for the clay-rich wearing course.

To achieve the desired results a very high percentage of cohesive clay-rich material is added to the wearing surface. An aggregate with a good particle size distribution from coarse (typically -3/4 inch) to very fine is modified to bring the -200 mesh (-75 μ m) content to ~30 wt% of the total material (Table 1). This is accomplished by mixing in material from a local cohesive clay-rich deposit; Penner pit clay was used for the RMC roads, and site 13 in the RM of Elton was the clay source for the Pioneer and Patricia roads (Figure 1, Table 2). The particle size distribution from coarse to micron-sized silt is important for maximum densification and bonding. The goal is to have every pore space occupied by progressively finer material. Ultimately any remaining space is occupied by micron to sub-micron sized cohesive clay particles that lock everything firmly in place through electronic bonding (Figures 5 and 6). The clay deposit must contain a high percent of cohesive clay such as smectite, montmorillonite, illite etc. Any clay material may be used provided it is in a sufficiently reactive state. In effect, clays with a high CEC have the potential for overall stronger inter-grain cation bonding. For construction purposes this equates to a high plasticity index (PI), which should be on the order of 12 or higher for the clay deposit, and >10 for the aggregate-clay mix. The material must also plot on or above the A-Line on the Casagrande plasticity chart, which essentially classifies the soil as a clay deposit rather than silt. The high-clay road material can be mixed and prepared in a quarry and brought to site as in this study (Figures 7A, B), or under appropriate circumstances the wearing course can be prepared on site, in-situ, by mixing in clay or aggregate to the existing road surface.

Once prepared in the quarry, the material is brought to site and windrowed (Figure 7B). Moisture content is checked, and then the material is laid down in 3 or 4 lifts, to which water and catalysts are added, and the material is brought to near optimum moisture content (OMC, Figure 7C). The catalyst used in this study is EarthZyme, an environmentally safe product which is solely manufactured by Cypher Environmental Ltd. It is an organic product comprising a proprietary blend of enzymes, electrolytes and surfactants. The catalyst acts as a densifying agent, facilitates water removal, increases the available cationic budget and facilitates clay bonding. The material is then rolled with graders back and forth across the road to thoroughly mix the aggregate, clay, water and catalyst (Figure 7D). The road surface is then shaped and compacted to a finished wearing surface of 15 cm to 20 cm thickness (Figures 7E, F). Once material is windrowed on site, final construction proceeds at the rate of 1 to 1.5 km per day, given that standard construction equipment including two graders, water truck, vibratory steel drum

compactor and a rubber tire roller are available. This requires roads to be closed for a maximum of one day. Roads are opened to traffic immediately upon completion of compaction. A detailed description of the materials preparation, construction and testing protocols are available by referring to Mumin and Cram, 2020.

Road Performance

Once constructed, these are non-gradable roads. They undergo a maintenance protocol of approximately once yearly or in some cases less. Maintenance requires a period of road softening by soaking overnight with water, or following a significant period of rain. After softening, the surface is scarified (generally with difficulty) to a depth of ~3 cm to 5 cm, and then reshaped and compacted, which completes maintenance for another year. Catalyst is generally not added during maintenance.

Curries Landing Road (CLR) in the Rural Municipality of Cornwallis (RMC) is a good example of the performance of an unpaved road stabilized by this technique. It was the most difficult, problematic and costly road to maintain in the RMC. It services ~ 10 active gravel quarries and carries ~200 to 250 fully loaded gravel trucks daily plus local residential traffic. It required near daily maintenance including constant watering, grading, chloride applications, addition of new material, and at the time this stabilization project commenced it was scheduled for reconstruction with provincial government financial assistance. In addition, one of the worst problems of this road for the RMC was the chronic and severe complaints from local residents about dust, wash boarding and potholes.

One mile of the CLR was reconstructed and stabilized in 2015 (Figures 2, 7B, 8, 9), and a further 2 miles in 2017. Lori Road, with high residential traffic was also stabilized in 2015 (Figures 7C, D, E, F, 10). After initial construction, the stabilized surface undergoes a period of curing, drying and further compaction from ongoing traffic that may take up to 30 days or more depending on traffic load and weather conditions. Further compaction during curing occurs due to the gradual removal of water upon drying, which leads to pore space that is ultimately removed by the constant compaction from traffic. Ultimately, these roads reach a highly compact, strongly bonded, durable semi-solid to semi-ductile state that easily supports the heaviest traffic conditions. For these roads, the heavier the traffic the better, as maximum compaction enhances the densification and bonding of the clay-rich wearing surface, which provides great bearing strength and strongly inhibits water ingress. The stabilized CLR road surface is shown again in 2018 and 2019, with no notable change in look or performance after 5 years (Figures 8, 9). The wearing surface remains in similar condition to the original construction, with the exception of moderately higher aggregate density in the upper 2 cm to 4 cm. This is attributed to embedding of fugitive gravel, and to minor loss of fines over time. It is not yet known when new material and/or product (catalyst) may need to be added to the road, as the service life of the wearing surface had not been reached at the time of writing this article.

Dynamic cone penetrometer (DCP) tests were conducted during year two of the stabilization project along the 1.6 km length of CLR, 1.6 km length of Lori Road, and 0.8 km length of Baker Road (all in RMC, Figure 11). They gave a range of California bearing ratio values (CBR) from 42% to 103% for the CLR (average 76% n = 6), 37% to 73% for Lori Road (average 51%, n=6;), and 72% to 133% for Baker Road (average 106%, n=6). For Lori Road, this represents an increase from an average 41% CBR taken 19 days after construction. Patricia Ave in Brandon was tested in 2016 (unstabilized), and again in 2018 one year

after stabilization. It had an average CBR value of 49.8% over 1 km of unstabilized road (n=12), and a high average CBR value of 219% (n=3) in 2018 one year after stabilization. Pioneer Road in the RM of Whitehead had an average CBR of 77% on Aug. 31, 2018, 27 days after stabilization (See Cram 2020, for details). The variability in bearing strength (CBR) is due to variable amounts of initial compaction during construction, varying traffic loads, different materials for Pioneer Road, material inhomogeneity, and variances in moisture content at the time of testing. This is consistent with laboratory testing of clay slabs, and standard laboratory CBR tests which show a direct and significant variance in semi-confined compression strength and CBR values as a function of increased compaction, length of curing, material compositions and moisture content at the time of testing (Gaboury 2015; Cram 2020). Nuclear densometer tests performed in 2015 by Manitoba Infrastructure after construction of Lori Road (RMC), averaged 106% of maximum dry density (Figure 12). To date frost damage is non-existent in any of the clay stabilized roads, in spite of Manitoba weather extremes that can range from -40°C to +40°C. Wash boarding and pot holes are also eliminated to the extent that maintenance is reduced to the once yearly protocol. Aggregate loss and dust generation are minimized due to the strongly bonded and durable surface. Dust tests using collection pots on Lori Road over a 3 day period, and a Turnkey Dust Mate environmental monitor on Pioneer road (two passes) showed a 77% (Lori Road) and 99% (Pioneer road) reduction in dust as compared to untreated sections of the same road (Gaboury, 2015; Cram, 2020). Although dust generation is highly variable on the same road depending on weather and traffic conditions, it is dramatically reduced in all cases. On April 20, 2020, ~300 days since last maintenance, CLR had a total defect score of 16 out of a maximum of 275 (Figure 2). For haul roads, maintenance is not considered imminent until a defect score between 60 to 130 is reached (see Thompson et al., 2019).

Composition and Mineralogy of Clay Deposits from Southwestern Manitoba

The remainder of this paper discusses the properties of clay deposits as relates to their suitability for use in road stabilization as described above. Materials investigated are derived from a 190 km by 225 km region of southwestern Manitoba, extending from the US border north to Dauphin, and from Portage la Prairie west to Virden (Figure 1). Materials were collected mostly from existing quarry sites designated as “clay pits” by the Manitoba quarries registry. Of twenty-nine sites examined, only 16 contained what could be classified as clay deposits, from which approximately 10 Kg samples were taken for analysis (Figure 14). All samples are from near surface glacio-lacustrine and glacio-fluvial materials deposited during retreat of the Laurentide ice sheet (Condrón and Winsor, 2011; Teller, 1976; Michalyna et al, 1976; Teller et al., 1996). The deposits are relatively thin layers comprising < 1 meter to several meters thickness. No attempt was made to determine the consistency or areal extent of any of the deposits.

The standard material against which the 16 deposits are compared is Penner clay (PC). Its performance in stabilized road construction in the RMC is well known, and its geotechnical properties are documented in our laboratory investigations (Gaboury, 2015; Cram, 2020). PC is taken from a location near the Assiniboine river ~ 7 km east of Brandon in the RMC, is comprised of ~ 91% material passing - 200 mesh and has a PI of ~19. It is mostly fine silt comprised of quartz, feldspar and carbonate, with a true clay mineral component of only ~25.2 %, dominantly montmorillonite, illite, kaolinite and chlorite. The silty nature of the clay deposit is important for construction, as it renders the material workable.

The 16 clay deposits that were sampled are highly variable in composition and properties. Petrographic examination was carried out with a NIKON E600 polarizing microscope in both transmitted and reflected

light for texture and mineral association. X-ray diffraction analyses (XRD) of the -400 mesh fraction (-37.5µm) was carried out for mineral identification and semi-quantitative abundance using a Rigaku MiniFlex 6G X-ray diffraction system equipped with a CoK α cathode tube, operated at 40kV and 15mA, 5° incident and receiving soler slits, 1.25° divergent slit, 2 θ range of 4°-90° and a D/teX Ultra2 detector. Mineral chemistry, and further mineral identification refinements were carried out using a JEOL 6390LV scanning electron microscope (SEM) equipped with an Oxford Instruments Ultim Max 100mm² silicon drift detector for energy dispersive spectroscopy, operated at 20Kv. The depth of analytical influence of the electron beam is several microns (Gill, 1997). SEM spot analyses were carried out on material identified by microscopy, SEM imaging, and by chemistry as clay mineral clots. However, they are mini-bulk analyses of multiple mineral grains due to the micron and sub-micron size of clays, which can be as little as 3 nanometers in thickness, and may in part be comprised of mixed layer clays (Holtz et al., 2011). Mineral composition is derived from the chemical analysis by employing a process of devolving the chemistry, similar to the process for calculating CIPW norms, but specific to SEM data and clays in this study (Jungen, 2020). Both XRD and SEM compositional data are semi-quantitative.

While analysis of the non-clay fraction is relatively straightforward, routine analysis of the mineralogy and chemistry of the clay is difficult. The micron and sub-micron grain size, and large chemical variation that occurs within individual mineral species, all create their own issues. Thirty-micron thick polished thin sections were made from -200 mesh material dried to ambient room conditions, and used for petrographic and SEM analyses. Thin sections were made according to procedures given by Camuti and McGuire (1999). Under conditions at Brandon University, dry clay deposit material including the clay slabs retain about 3% adsorbed moisture, which varies somewhat according to ambient temperature, humidity, texture, amount and type of clay minerals present. In thin section, the clay occurs largely as flocculated clots up to 75µm in size, with clots comprising up to 10,000s of micron to submicron (nano-particles) mineral grains. Embedded in the clay clots are numerous micron to submicron-sized particles of other minerals including quartz, carbonate and feldspar (Table 2, Figure 15). The extremely fine micron and nano-particles present in these clays are believed to result from a combination of weathering and glacial pulverization.

XRD analysis for the 16 clay deposits sampled in this study shows between ~7.5-38.8 wt% total clay minerals. The remaining 61.2-92.5 wt% is comprised of silt, including abundant sub-micron particles. The silt fraction of the clay deposits is comprised of quartz (0.0-30.3 wt% of the total sample mineralogy), feldspar (3.7-27.0 wt%), carbonate (0.0-76.2 wt%), mica (0.0-18.1 wt%), zeolite (0.0-6.5 wt%), amphibole (0.0-5.3 wt%), and other minerals (0.0-7.3 wt%) (Table 2). The clay mineral fraction of the 16 samples is comprised of illite (0.4-31.4 wt%), montmorillonite (0.0-5.9 wt%), chlorite group minerals (0.5-17.2 wt%), kaolinite group minerals (0.0-12.0 wt%), and vermiculite (0.0-6.0 wt%), and other clays (0.0-2.1 wt%, Table 2). By contrast, Oscarson and Dixon (1989) determined that one glacio-lacustrine deposit from near Winnipeg, MB had a high clay content of approximately 30-40 wt% smectite, 15-25 wt% illite, 5-15 wt% kaolinite, 10-20 wt% quartz, 5-10 wt% calcite, and minor amounts of feldspar and dolomite. Montmorillonite and vermiculite are the most reactive (highest potential -ve charge and highest CEC), followed by illite, chlorite, and then kaolinite group clays which are the least reactive (Holtz et al, 2011).

SEM analyses were performed on clotted particles of clay-rich materials (Figure 15), which gave composite results for multiple micron and sub-micron grains. From 1,243 analyses, only 89 were selected as least contaminated with non-clay material, averaged, and devolved into mineral composition

(Jungen, 2020; Table 2). The high montmorillonite content is presumed due to its highly reactive state, and tendency to flocculate into the clots that were analyzed. It is also possible that during devolution of the chemical analyses, montmorillonite may be overestimated at the expense of carbonates, and chlorite somewhat overestimated at the expense of vermiculite.

Engineering Properties of Southwestern Manitoba Clay Deposits

Engineering properties were determined by standard Atterberg's tests (ASTM D 4318 2005) on the -40 mesh fraction of the clay deposits by using a cone penetrometer, a liquid limit machine, and a rolling device for plastic limit tests. From this are derived the plasticity index (PI) of the materials, giving a relative indication of the materials cohesiveness (Table 2). The liquid limit of the 16 clay samples varied between 18.6 and 56.9% moisture, and the plastic limit between 13.5 and 30.9% moisture (Toews, 2020). The resultant plasticity index range varied from 5 to 28 (Table 2).

The utility of the clay-rich material for stabilization is estimated also from their relative bonding and strength characteristics. This was carried out using semi-confined compressive strength tests on 2.5 inch diameter slabs constructed for the purpose of this study. Clay slabs were constructed from 120 grams (dry weight) of -10 mesh (-2mm) material. They were brought to near OMC, catalyst added in the same amount as for road construction, compacted at 2000 PSI for 5 minutes, and cured/dried for 7 days between two sheets of gypsum board at $\sim 20^{\circ}\text{C}$. The slabs were then placed under compression in a 10,000 lb load frame with a one square inch surface area button piston and put under strain at 200 μm per minute until failure (maximum semi-confined compressive strength) was reached. This method facilitated laboratory testing of hundreds of samples with varying parameters, providing a comparative indication of the behavior of different clay-rich materials under load (Figure 13).

The semi-confined compression strength of clay slabs from each of the 16 clay deposits as well as Penner clay is listed in Table 2. The corresponding PI and wt % of clay minerals present are also given. The semi-confined compression strength ranges from ~ 1779 to 4947 PSI, which provides a relative measure of the degree and strength of electronic bonding (electrostatic attraction) between the clay minerals and inter-particle cations, in combination with any other inter-particle physical and/or chemical reactions. For the clay deposits from southwestern Manitoba, high compressive strength generally correlates with high PI and the amount of cohesive clay minerals present in the samples, although exceptions occur that relate compositional and textural variations between deposits.

Standard 6" cylinder laboratory CBR tests are not suitable for testing high-clay road materials used in this investigation. The high-clay content retains significant and highly variable amounts and distribution of moisture in the CBR cylinders, which do not dry uniformly over 7 days. This dramatically and variably alters the materials CBR, and is not representative of what occurs in an actual road. Both increased curing time (decreased moisture content) and compaction energy result in a dramatic increase in compressive strength, until a maximum is reached (Figure 16). In practice, roads constructed with high-clay contents undergo a curing period under traffic load, during which moisture content decreases while compaction, density and strength continue to increase.

Discussion and Conclusions

This investigation demonstrates that durable, high-functioning, low maintenance, cost effective and environmentally sustainable unpaved roads can be routinely constructed or stabilized by taking advantage of the small size and unique electronic bonding potential of cohesive clays. The same properties that result in extensive water adsorption and loss of strength are harnessed to create high densification, impermeability, and strong electronic clay mineral bonding. Best results are achieved using aggregate with a broad particle size distribution, a high amount of cohesive clay, catalytic agents, natural occurring cationic polymers, and the appropriate construction protocol.

A broad particle size distribution from coarse to sub-micron grains facilitates maximum densification. Micron and sub-micron particles of cohesive clay and ultra fine silt occupy any remaining pore space and coat larger fragments. Strong electrostatic forces bond clay particles in the absence of water and presence of cationic polymers causing clay to cement the aggregate firmly in place. Construction of these high-clay roads requires its own unique but simple construction protocols, testing and monitoring.

Several unique and important properties are inherent to roads stabilized by this method. High densification and bonding of the clays imparts a strong resistance to water ingress, allowing efficient water shedding and limiting retained moisture. These roads remain in a semi-ductile to semi-solid state with high bearing capacity and very strong compressive strength that strongly resist formation of potholes, rutting, wash boarding and frost damage. In spite of the temperature extremes experienced in the Canadian prairies that can reach -40°C in winter to $+40^{\circ}\text{C}$ in summer, no frost damage occurs in any of the stabilized roads in the project area. During the curing period and over time, moisture removal and continuous compaction by high traffic volumes lead to further increases in density and bearing strength.

Another unique feature of the high cohesive clay content is that it imparts a ductile and self-healing nature to the roads. Within the first few days to weeks after construction, minor cracking may occur as a fine spidery network or occasional larger cracks. This is due to shrinkage during the initial drying/curing phase as water is removed, resulting in pore space. However, within a short period of generally a few days to weeks, evidence of cracking disappears with a complete apparent healing (re-bonding), helped by continued traffic induced compaction that removes the pore space. There has not been any negative effect on road performance due to any initial cracking. A version of the phenomenon of cracking and healing occurs in the laboratory during drying of clay slabs. Typically, after a day or so of drying, radial shrinkage cracks occur in the slabs. These cracks, even when prominent, entirely disappear by day four or five of the drying, leaving no evidence of their prior existence. It appears that the clay slabs are electronically re-bonding, even after significant separation has occurred.

Clay deposits throughout much of the Prairies, Ontario, Quebec and parts of the northern US are largely glacio-lacustrine and/or glacio-fluvial in origin. However, much of the clay minerals had their origin from weathering during interglacial periods. These deposits are widely distributed, typically irregular in morphology (Teller, 1976; Teller et al., 1996), and heterogeneous in composition. Clay mineral abundance in the deposits analyzed in this study is highly variable in amount, but comprised largely of a mixture of 5 clay groups being illite, smectite (montmorillonite), chlorite, kaolinite and vermiculite. Illite, montmorillonite, kaolinite and vermiculite are primarily the result of weathering, while chlorite is most likely residual from the original rock, having formed due to ancient metamorphism and metasomatic processes that affected primary rocks long before glaciation (Hugget, 2015).

The bulk of the clay deposit material tested in this study is comprised of quartz, feldspar and carbonate minerals as sand, silt and micron to sub-micron sized particles. The presence of this non-clay silty material is beneficial to the road stabilization process in that it helps with the densification and bonding, and renders the clay deposit workable during the materials preparation (mixing) and construction process. Stabilized roads in the project area have clay mineral abundance in the final road mix on the order of about 7 to 12 wt%, while the -200 mesh fines content ranges between ~20 to ~40 wt% of total wearing surface material. This requires that as much as ⅓ of the wearing surface (dry weight basis) is derived from the clay deposit, rather than a gravel quarry. Along with all the benefits to road functionality, safety, environment and vehicle wear, stabilization removes the need to continually add aggregate to the road, which can result in a major reduction in the use of high-quality aggregate resources.

The suitability of clay deposits for road stabilization from a large area of southwestern Manitoba was examined. The results are compared to the Penner clay deposit (PC) which is our standard material since its properties in the lab and its performance in actual road construction are well documented. The PI of Penner clay is ~19, and its standard semi-confined compressive strength under parameters used for this study is ~3,720 PSI. Any material that approaches these characteristics should be very good for stabilization.

The PI of the 16 deposits examined in this study ranges from 5 to 28, while maximum semi-confined compression strength varied from 1779 to 4947 PSI, with all except one greater than 2650 PSI. The deposits with highest PI (high cohesive clay content) also have high compressive strength, however, a lack of direct correlation occurs and is due to the compositional and textural heterogeneity between deposits. In particular, high carbonate contents also correlate with high compressive strength (e.g. samples 15, 28.5, 30; Table 2). The highest strength sample (28) has high clay content, high PI, and high carbonate content. We suspect that a combination of micron to nano-particles, along with treatment and compaction results in some recrystallization reaction involving ultra fine carbonate minerals. Correlation of high-strength with high PI is counter-intuitive since untreated clay-rich soils with high plasticity (PI) are known to be low strength construction materials (Holtz et al., 2011; Barnes, 2016; Thompson et al., 2019). While the PI is an indication of plasticity or cohesiveness of the clay deposit in a moist state, its semi-confined compressive strength is an indication of the relative strength of electrostatic bonding along with any other inter-particle reactions that occur, in a dry or cured state.

For stabilization purposes under conditions similar to southwestern Manitoba we recommend a PI not less than 12 for the clay-rich material added to an aggregate base. Thirteen of the 16 clay deposits tested meet this criteria, and 7 exceeded the semi-confined compressive strength of Penner clay.

In conclusion, highly effective bonding and stabilization of unpaved (aggregate) roads is possible with: 1) the input of high amounts of cohesive clay with high electrostatic bonding potential, 2) use of an aggregate having a good particle size distribution, typically from -3/4 inch to ultra fine (micron and smaller) material, 3) use of an organic catalyst to promote densification, water removal and bonding, and 4) appropriate construction and testing protocols. The overall composition of the road material impacts its bonding, strength and durability. Clay deposits suitable for the stabilization procedures outlined in this paper are widely available in areas with glacio-lacustrine and glacio-fluvial deposits left behind during retreat of the Laurentide ice sheet. This includes much of the northern and central

portions of North America, however, the results of this study apply to clays of any origin provided they are sufficiently reactive. If using the technologies presented here, we recommend thorough testing of local materials, and following the protocols for construction as outlined in this report and cited herein.

References

- ASTM D 4318, 2005. Standard Test Methods for Liquid Limit, Plastic Limit, and Plasticity Index of Soils
- Barnes, G., 2016. Soil Mechanics Principles and Practice, Fourth Edition, Palgrave.
- Camuti, S.C., and McGuire, P.T., 1999. Preparation of polished thin sections from poorly consolidated regolith and sediment materials. *Sedimentary Geology* Vol. 128, p. 171-178.
- Condron, A., and Winsor, P., 2011. A Subtropical fate awaited freshwater discharged from glacial Lake Agassiz, 1-5, doi:10.1029/2010GL046011.
- Cram, R., 2020. The Stabilization of Unpaved Roads Using Cohesive Clays and Organic Catalysts. M.Sc. Thesis, Brandon University, submitted.
- Gaboury, G.A., 2015. Bio-stabilization of unconsolidated base materials. Honours Thesis, Brandon University, pp. 90.
- Gill, R., 1997. Editor, *Modern Analytical Geochemistry: An Introduction to Quantitative Chemical Analysis for Earth, Environmental and Materials Scientists*. Longman, pp. 329.
- Güven, N. 1992. Molecular aspects of clay-water interactions, *in* N. Güven and R. M. Pollastro (eds), *Clay-Water Interface and its Rheological Implications*, CMS workshop lectures, Vol. 4, Clay Minerals Society, Boulder, CO, p. 2-79.
- Holtz, R.D., Kovacs. W.D. and Sheahan, T.C., 2011. *An Introduction to Geotechnical Engineering* 2nd Edition, Pearson Education Inc.
- Hugget, J.M., 2005. Clay Minerals. *Encyclopedia of Geology*, p. 358-365.
- Jungen, G., 2020. Nature of clays in southwestern Manitoba, and their use for unpaved road stabilization. Honours Thesis, Brandon University.
- Klein, C., and Dutrow, B., 2007. *Manual of Mineral Science*, 23rd Edition. John Wiley and Sons Inc., pp 716.
- Michalyna, W., Podolsky, G.P. and Gardiner, W., 1976. *Soils of the Brandon Region Study Area*, Manitoba Department of Municipal Affairs, Municipal Planning Branch.
- Mitchell, J.K., and Soga, K., 2005. *Fundamentals of Soil Behaviour*, 3rd Edition. John Wiley and Sons Inc., pp 577.
- Mumin, A.H. and Cram, R., 2020. *Manual for Clay Stabilization of Unpaved Gravel Roads: Materials and Procedures*. Brandon University.
- Oscarson, D. W. and Dixon, D. A., 1989. Elemental, mineralogical, and pore-solution compositions of selected Canadian clays, Chalk River, Ontario.
- Sogami, I. and Ise, N., 1984. On the electrostatic interactions in macroionic solutions, *Journal of Chemical Physics*, Vol. 81, p. 6320-6332.
- Teller, J.T., 1976. Lake Agassiz Deposits in the Main Offshore Basin of Southern Manitoba, *Can. J. Earth Sci.*, Vol. 13-1, 27-43.
- Teller, J.T., Thorleifson, L.H., Matile, G., and Brisbin, W.C., 1996. Sedimentology, geomorphology and history of the central Lake Agassiz basin. *Geological Association of Canada Field Trip Guidebook*, pp.108.

Thompson, R.J., Peroni, R., and Visser, A.T., 2019. Mining Haul Roads: Theory and Practice. CRC Press, Taylor and Francis Group, pp. 294.

Toews, Z., 2020. Analysis and suitability of various clays from southwestern Manitoba for use in road stabilization. Honours Thesis, Brandon University.

Transport Canada, 2008. Transportation in Canada 2007: An Overview, Addendum, Catalogue no. TP 14816E, p. A85.

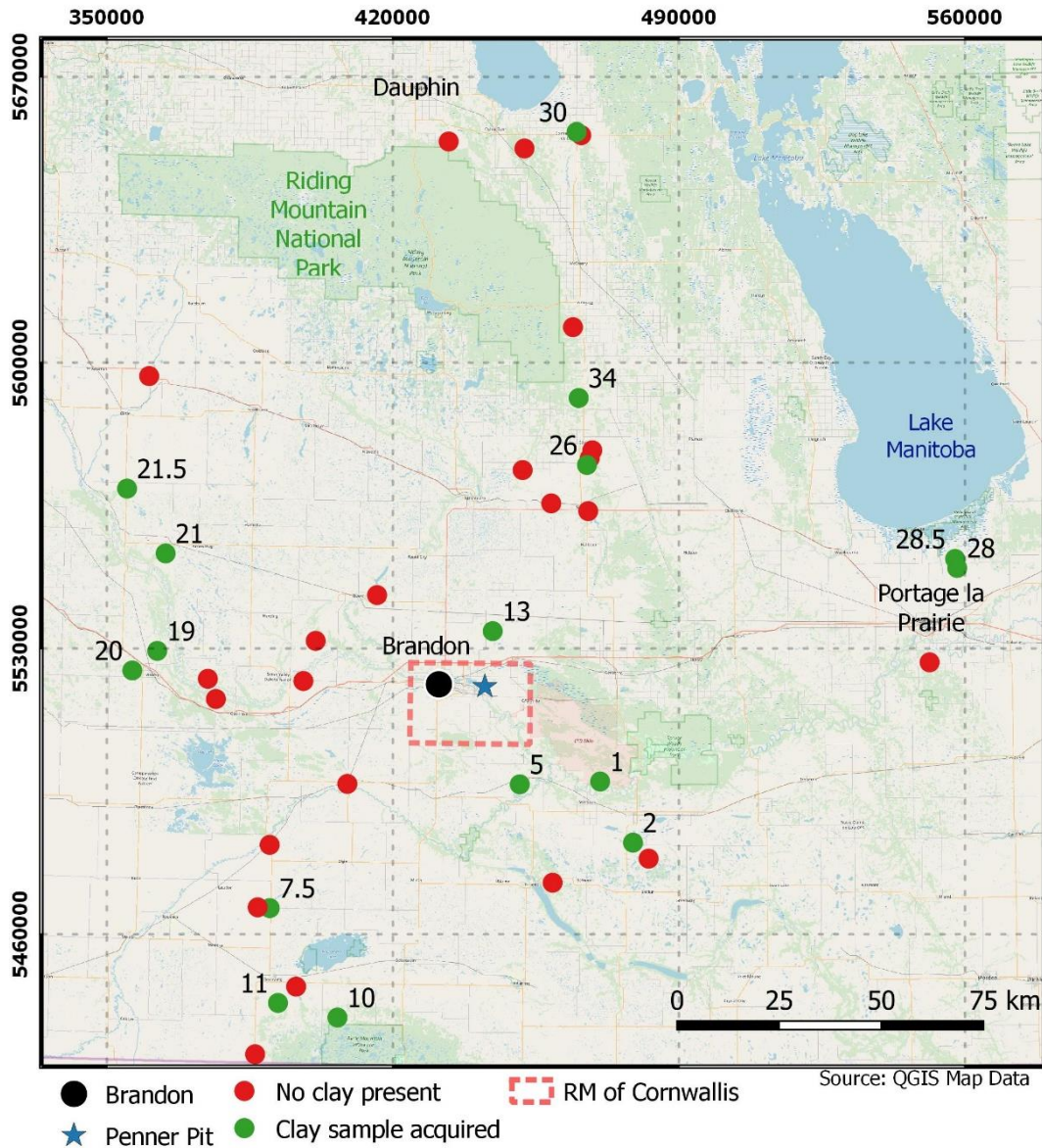


Figure 1: Project sample location map in southwestern Manitoba. Red dots were quarries classified as clay pits that did not contain clay rich materials, however, it does not exclude the probability of nearby clays deposits which is the norm for the region. Base map source is QGIS Map Data, Natural Earth.



Figure 2: Curries Landing Road after stabilization in 2015 (top left), and in April 2020 (top right). Pioneer road after stabilization in 2018 (bottom).

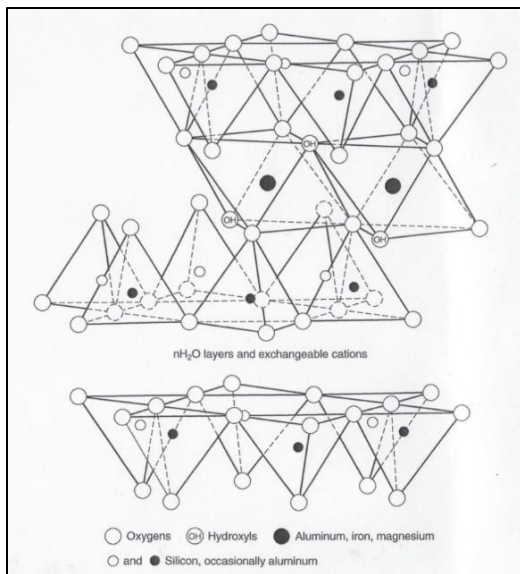


Figure 3: Atomic structure of montmorillonite showing tetrahedral (Si⁴⁺), and octahedral (Al³⁺) sites where substitution by lower-valent cations occurs and excess negative charge originates (Grim 1959).

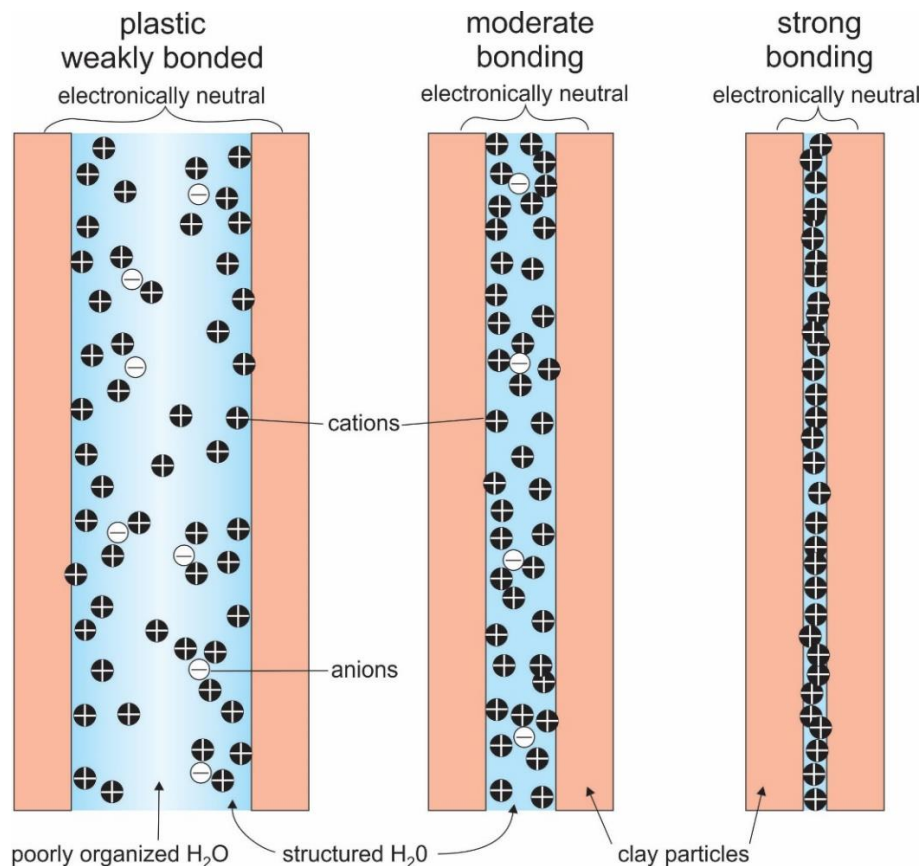


Figure 4: Bonding of clay particles with excess negative charge distributed along surfaces. An overall electronically neutral state occurs at all stages. When naturally occurring \pm introduced cations dominate the inter-particle bonding without significant water, clay particles are held together by strong electrostatic forces. Thickness of clay particles is ~ 3 to 30 nanometers, long dimension up to ~ 2 microns.

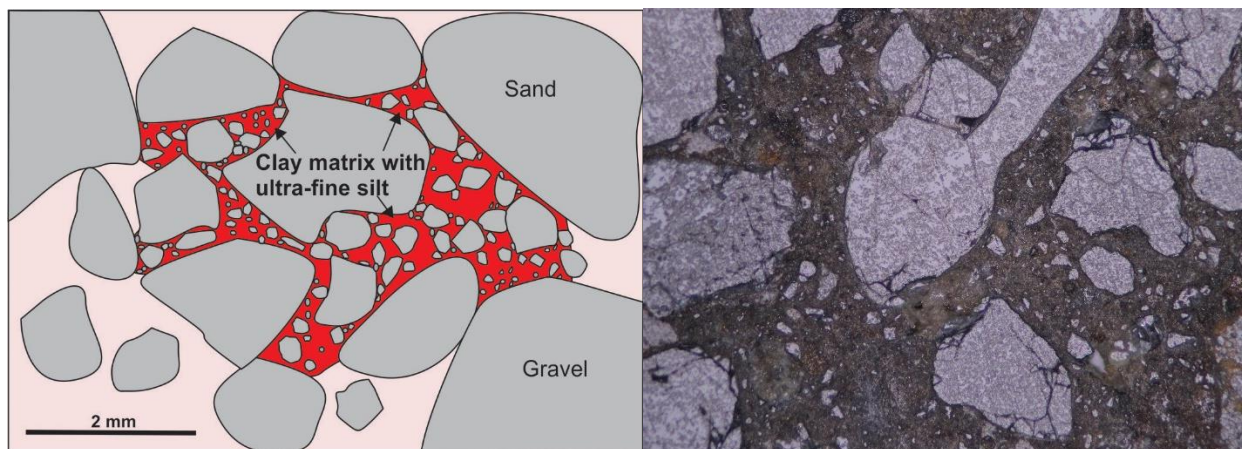


Figure 5 (left): Maximum densification and bonding occurs when all pore spaces are filled by progressively finer particles, with remaining space occupied by micron and sub-micron size cohesive (reactive) clay and ultra-fine silt (red). Locking occurs when clay particles electrostatically bond. Figure 6 (right): Photomicrograph of a thin section cut from a road block similar to that shown in Figure 8, showing sand and silt well cemented in a clay-rich matrix. Larger clasts are quartz, feldspar and carbonates. Reflected polarized light, f.o.v. = 2mm.

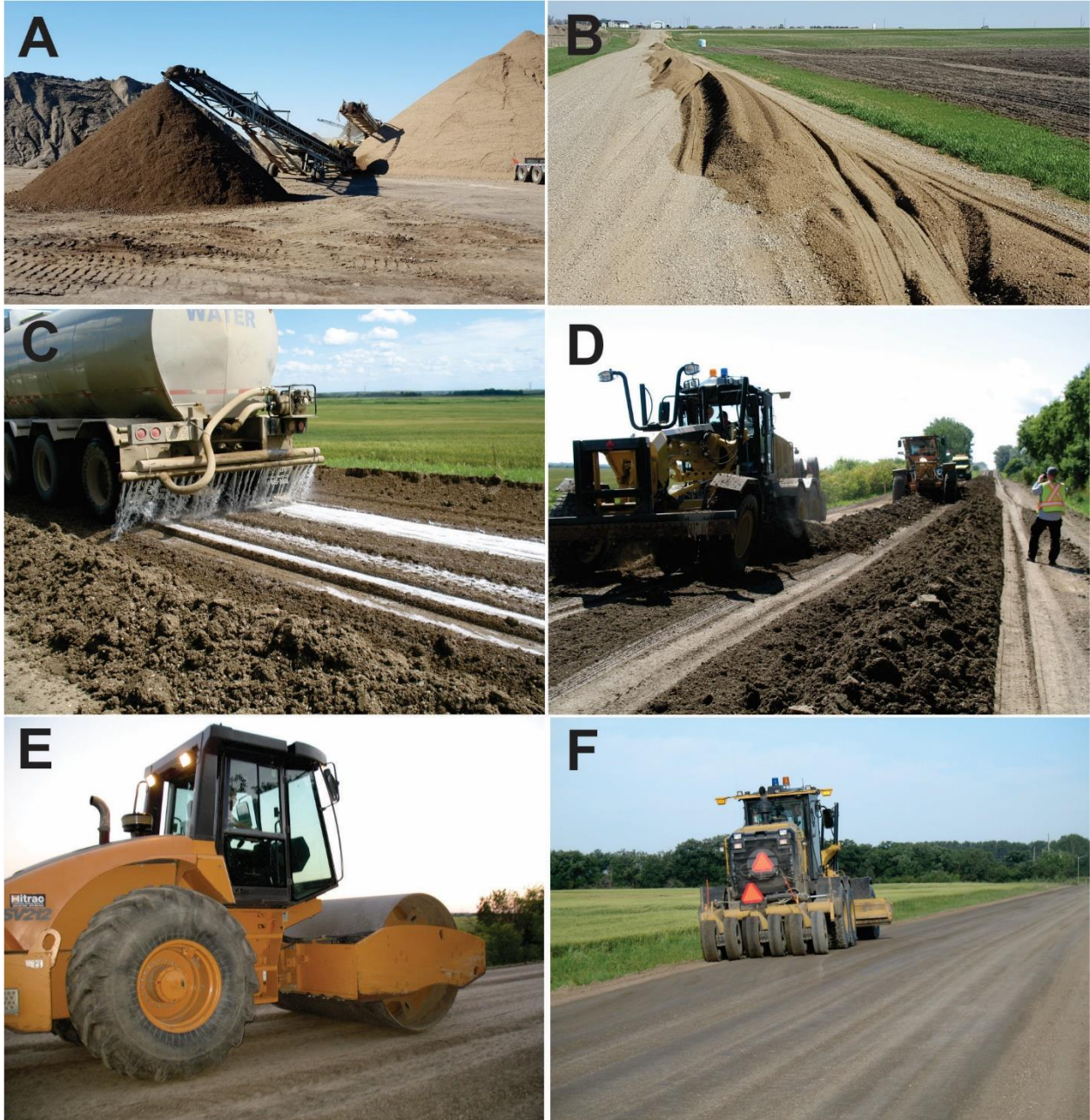


Figure 7: The construction sequence for stabilization of unpaved roads in the RM of Cornwallis. A) in-quarry mixing of an A-base aggregate with a cohesive clay deposit. B) Windrowing material prior to construction, Curries Landing Road. C) Adding water with EarthZyme densifier and catalyst to reach near OMC. D) Blading material back and forth across road to mix water, catalyst, clay and aggregate. E) Compacting with steel drum roller. F) Application of final slurry coat, sealing and finishing with rubber wheel compactor. C, D, E, F from Lori Road. Construction by Bluestar Construction.



Figure 8 (left): Block cut from Curries Landing Road in 2018. Figure 9) Wearing surface of CLR during the 5th year of road life, summer of 2019. The road maintains a well-bound pebbled surface. Wearing surface is 20cm thick and comprised of A-base aggregate plus Penner clay mixed to ~32% -200 mesh fines resulting in ~10% clay minerals in the final mix.



Figure 10: Lori Road after stabilization and reconstruction with a 15cm thick wearing surface of A-base aggregate plus Penner clay mixed to ~32% -200 mesh fines resulting in ~10% cohesive clay minerals in the final mix. Left) Zach Toews using a concrete saw to cut blocks for examination and testing. Right) Profile through Lori Road in 2018, 3 years after stabilization.



Manitoba		P.R. - P.R.	205	KILOMETER	REGION	93						
Soils / Granular Density Report		ZONE	0450	LIFT	CONTRACT	WALLEY						
Test Type	TEST	STA.	Sta.	LINE	PRODUCT	CONTRACTOR						
		0+50	0	0	Base Course C-Drawn							
Stage #	Y-2	Station	0+50	0+50	2+50	4+50	6+50	8+50	10+50	Probe Position		
D. Moisture Count		0	0	0	0	0	0	0	0	BS		
D. Density Count		0	0	0	0	0	0	0	0	BS		
		Offset	ES	C	WS	ES	ES	C	WS	WS		
		Number	1	2								
Moisture kg/m ³ (1)		142	138	155	150	145	159	144	124	153	150	AVG
Moisture kg/m ³ (2)		142	149	161	152	136	160	150	126	149	146	A
Average Moisture kg/m ³	A	2393	2344	2366	2361	2411	2401	2407	2291	2311	2401	A
Moisture Correction	B	1,000	1,000	1,000	1,000	1,000	1,000	1,000	1,000	1,000	1,000	B
Moisture Content % (AxF)	C	142	144	158	151	141	160	147	125	151	149	C
Dry Density kg/m ³	V											V
Dry Density kg/m ³ (M)												M
Wet Density kg/m ³ (1)		2329	2264	2250	2364	2258	2254	2300	2206	2295	2327	AVG
Wet Density kg/m ³ (2)		2388	2204	2281	2360	2251	2341	2295	2205	2292	2327	D
Avg Wet Density kg/m ³	D	2393	2344	2366	2361	2411	2401	2407	2291	2311	2401	D
Dry Density kg/m ³ (D-C)	E	2191	2091	2105	2211	2154	2088	2151	2081	2143	2170	E
Proctor 2013 Optimum 9.3%	F	2033	2033	2033	2033	2033	2033	2033	2033	2033	2033	F
% of Proctor (E/F) x 100	G	107.7%	102.8%	103.7%	108.8%	104.0%	102.7%	105.8%	102.3%	105.4%	107.0%	G
% Moisture (E/B) x 100	H	6.6%	6.6%	7.6%	6.8%	6.6%	7.4%	6.8%	6.0%	7.0%	6.8%	H
Location that will be retested												
# Tests	10	Moisture Correction Formula		Average		Accept	Overall		Pass			
Spic	58%	M x D		Table T1		N/A						
Table T1		A = (B x A)		Spec 506.2.7.6.1								

Figure 11 (left): Riley Cram conducting DCP CBR testing of Baker Road in 2018, 3 years after stabilization. Average CBR = 106%. In year 6, 2020, the road remains in excellent condition. Figure 12 (right): Aaron from Manitoba Infrastructure (right) and Greg Gaboury of Brandon University (left) conducting nuclear densometer tests on Lori Road August 24, 2015, one month after construction. Average dry density was 105% of maximum with OMC = 9.3% (n=10).

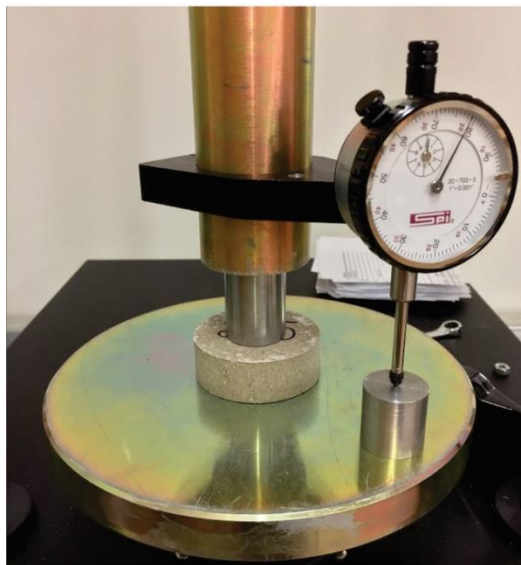


Figure 13: Semi-confined compression tests on 2.5" diameter clay slabs with a 1 square inch surface area button piston (left). Clay slabs after testing. Maximum compressive strength recorded at failure.



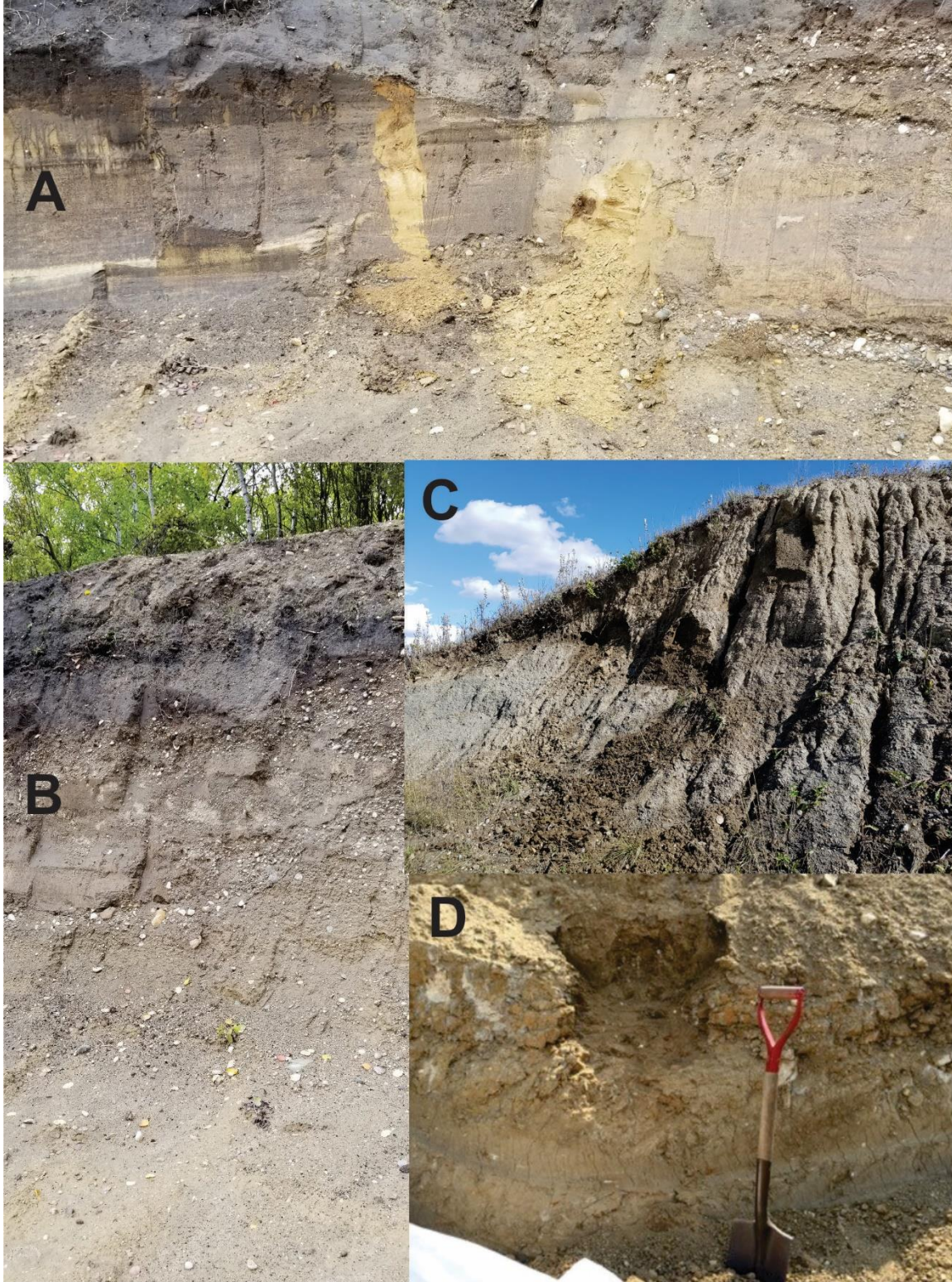


Figure 14: Four of the Manitoba clay deposits tested in this study. A = Rural Municipality (RM) of Prairie View sample 21. B = RM of Prairie View sample 21.5. C = RM of Deloraine-Winchester sample 7.5. D = RM of Elton sample 13. Stony clasts in all photos are mostly dolomite and limestone.

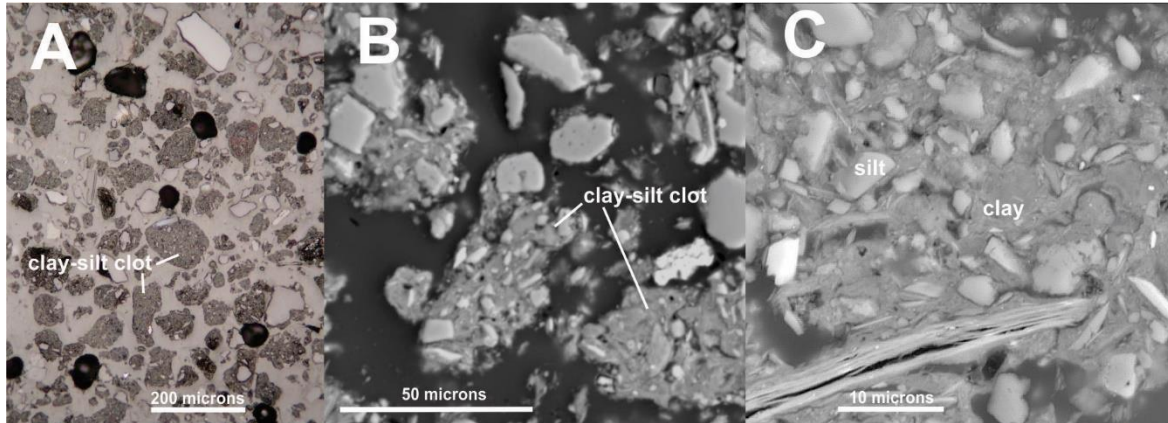


Figure 15: Reflected light image (A) showing clay clots with embedded micron and sub-micron silt particles (grey fuzzy patches, sample # 10). SEM BSE images (B #10 and C #13) of clay clots (clay = medium grey matrix) with embedded silt (brighter). Angular silt grains formed by glacial pulverization.

15: Reflected light image (A) showing clay clots with embedded micron and sub-micron silt particles (grey fuzzy patches, sample # 10). SEM BSE images (B #10 and C #13) of clay clots (clay = medium grey matrix) with embedded silt (brighter). Angular silt grains formed by glacial pulverization.

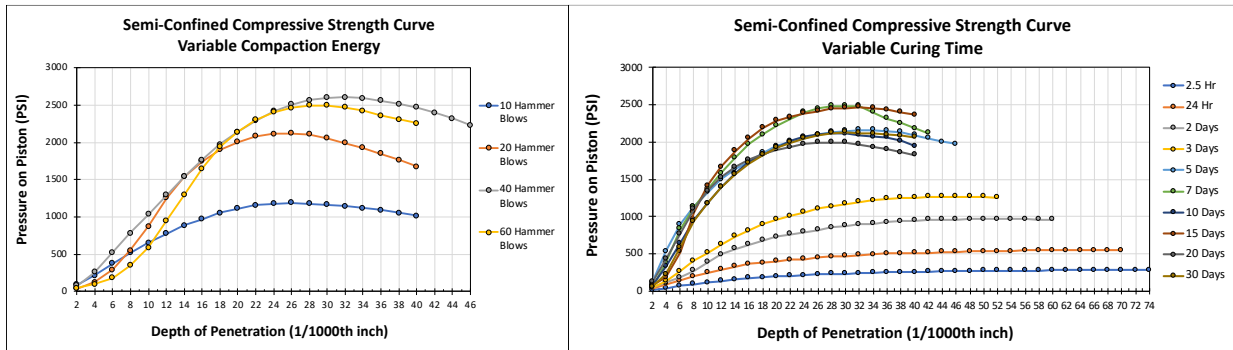


Figure 16: Effect of increasing compaction and curing time on semi-confined compressive strength for Penner clay slabs treated with organic catalyst. Compaction was from a 5.5lb-f (24.4-N) proctor hammer. Maximum semi-confined compressive strength of ~ 2,500 PSI occurred at 40 hammer blows. Right) Clay slabs were compacted with 20 blows from a 5.5-lbf (24.4-N) proctor hammer. Maximum strength is reached on full drying to ambient moisture conditions, which occurred in ~5-7 days.

Particle Size Analysis (Sieve Test):						
Seive Time	Seive Size/Number	% of Total Sample (Retained)				
		Curries Landing (South), Baker Rd, Lori Rd average	Patricia Ave.	Curries Landing Rd. (South) Cut Out #1	Curries Landing Rd. (South) Cut Out #2	Curries Landing Rd. (South) Cut Out #3
15 minutes	1" (25.4mm)	0.00%	0.00%	0.00%	0.48%	0.00%
	3/4" (19.05mm)	1.40%	1.99%	0.00%	0.29%	0.00%
	3/8" (9.525mm)	8.84%	23.88%	18.75%	8.19%	16.50%
	1/4" (6.35mm)		7.82%		6.21%	
	No. 4 (4.75mm)	9.04%	4.84%	18.59%	4.18%	17.80%
15 minutes	No. 10 (2.0mm)	9.88%	8.83%	11.60%	7.92%	11.70%
	No. 20 (0.841mm)	9.66%	5.77%	5.04%	4.06%	6.10%
	No. 40 (0.420mm)	11.60%	7.59%	6.02%	5.04%	8.70%
	No. 60 (0.250mm)	9.94%	5.14%	7.03%	5.40%	
	No. 100 (0.149mm)	3.66%	2.83%	2.93%	3.13%	12.60%
	No. 140 (0.105mm)	2.09%	1.65%	1.36%	3.19%	
	No. 200 (0.075mm)	1.75%	1.45%	1.55%	4.23%	3.00%
	<No. 200	32.26%	28.25%	26.86%	47.65%	23.60%
Collected Weight (g)		100.11%	100.04%	99.73%	99.97%	100.00%
% Lost During Seiving		-0.11%	-0.04%	0.27%	0.03%	

Table 1: Particle size distribution for stabilized roads in the RMC showing variable high fines content.

Table 2: Properties and mineral composition (wt %) of Manitoba clay deposits. XRD for bulk analysis, SEM for spot analysis of clay-clots. SCC PSI = semi-confined compressive strength in pounds per square inch. Mineral groups are colour coded. Tremolite and Actinolite are listed together.

Sample #	Penner	Penner	1	1	2	2	5	5	7.5	7.5	10	10	11	11	13	13	19	
<200 mesh	91%	91%	92%	92%	83%	83%	55%	55%	60%	60%	64%	64%	67%	67%	57%	57%	98%	
Plasticity Index	19	19	22	22	22	22	15	15	16	16	19	19	22	22	23	23	15	
SCC PSI	3720	3720	4778	4778	4497	4497	3291	3291	3911	3911	4105	4105	3287	3287	4153	4153	2654	
Method	XRD	SEM	XRD	SEM	XRD	SEM	XRD	SEM	XRD	SEM	XRD	SEM	XRD	SEM	XRD	SEM	XRD	
Type	BULK	SPOT	BULK	SPOT	BULK	SPOT	BULK	SPOT	BULK	SPOT	BULK	SPOT	BULK	SPOT	BULK	SPOT	BULK	
# of analyses	n=2	n=4	n=6		n=5		n=5		n=5		n=7		n=6		n=6			
Clay	Illite	3.4	16.6	5.6	18.3	16.0	24.0	2.5	24.7	11.3	25.3	8.4	20.2	16.8	26.8	7.3	19.2	31.4
Clay	Montmorillonite	16.9	33.8	3.3	37.4	1.6	19.3	0.0	13.1	1.6	19.6	1.8	39.2	3.7	29.3	0.1	22.3	0.0
Clay	Chlorite Group		0.8		14.4		12.8		17.2		13.2	0.5	11.3	3.1	9.5		12.4	
Clay	Chinochlore	1.6		0.5		14.0		1.4		6.5						13.3		
Clay	Chamosite			5.7					1.0									5.3
Clay	Vermiculite	0.2			0.0	4.7	4.4	0.3	2.9			2.6	0.8	0.5	1.4	0.4	1.4	
Clay	Kaolinite Group	2.8	13.7	8.5	18.3		20.8	2.6	24.3		21.3	7.1	10.1		21.9	8.3	28.9	
Clay	Lizardite																	
Clay	Dickite	0.4						4.4						0.7				
Clay	Nacrite													5.2		3.7		
Clay	Sepiolite																	2.1
	% Clay Minerals	25.2		23.6		36.3		11.2		20.3		20.4		30.0		33.1		38.8
Silicate	Quartz	24.8	30.9	27.8	11.2	30.3	18.6	10.3	14.0	21.7	15.6	20.1	9.9	16.7	8.1	14.8	11.0	19.8
Carbonate	Dolomite	18.0	1.6	5.4				59.0	2.6	21.9	2.7	25.9	3.1	33.4	2.9	27.2	4.0	16.2
Carbonate	Calcite	6.0	2.6	9.1	0.5	1.4		2.2	2.9	2.9	4.2	1.7	6.3	0.2	2.2	0.8	3.1	
Feldspar	Albite	9.6		26.3		24.7		4.4	1.2	15.6	2.3	18.1	3.7			10.6		9.9
Feldspar	K-Feldspar																	
Feldspar	Orthoclase																	
Feldspar	Anorthoclase	5.1																
Feldspar	Microcline	3.9				2.3				8.4		5.8						5.6
Feldspar	Oligoclase													12.0				
Amphibole	Hornblende																5.3	1.3
Amphibole	Tremolite	0.7						0.8										
Mica	Muscovite	5.5						9.5		5.1						3.7		3.2
Mica	Biotite																	
Mica	Phlogopite				4.6					3.1		5.6						
Silicate	Titanite																	
Zeolite	Clinoptilolite			2.1		4.4				0.9				0.9				
Zeolite	Mordenite	1.0						2.7								3.0		
Pyroxene	Diopside																	
Phyllosilicate	Talc																	2.2
Silicate	Cordierite			1.1										1.0				

Sample #	19	20	20	21	21	21.5	21.5	26	26	28	28	28.5	28.5	30	30	34	34	
<200 mesh	98%	55%	55%	96%	96%	42%	42%	55%	55%	84%	84%	50%	50%	62%	62%	48%	48%	
Plasticity Index	15	15	15	7	7	22	22	19	19	28	28	5	5	10	10	20	20	
SCC PSI	2654	3057	3057	1779	1779	3306	3306	3335	3335	4947	4947	4080	4080	3696	3696	3511	3511	
Method	SEM	XRD	SEM	XRD	SEM	XRD	SEM	XRD	SEM	XRD	SEM	XRD	SEM	XRD	SEM	XRD	SEM	
Type	SPOT	BULK	SPOT	BULK	SPOT	BULK	SPOT	BULK	SPOT	BULK	SPOT	BULK	SPOT	BULK	SPOT	BULK	SPOT	
# of analyses	n=5		n=3		n=6		n=5		n=5		n=7		n=5		n=5		n=4	
Clay	Illite	38.2	1.4	27.0	0.4	28.8	9.9	14.5	2.9	24.9	8.8	33.5	2.9	45.9	1.6	22.0	10.7	26.8
Clay	Montmorillonite	19.5	2.1	24.8	2.9	30.1	0.5	27.6	5.9	22.7	4.4	22.7	0.5	9.7	2.2	6.5	5.7	20.6
Clay	Chlorite Group	12.0	3.4	13.5		11.3		11.9		9.7		11.0		8.2		8.5	10.2	14.5
Clay	Chinochlore				11.6		5.1						4.1			3.8		
Clay	Chamosite								7.6		3.4							
Clay	Vermiculite	1.4		1.4		1.4	2.4	0.3		1.1	4.4	1.6		0.8		1.8		1.1
Clay	Kaolinite Group	23.9	3.3	12.2		11.0		0.2		12.6				2.7		32.0		9.7
Clay	Lizardite														1.5			
Clay	Dickite										10.7				2.7			
Clay	Nacrite										3.4							
Clay	Sepiolite					1.8												
	% Clay Minerals		10.3		16.7		17.9		16.4		35.1		7.5		11.9		26.6	
Silicate	Quartz	2.2	12.3	9.1	13.3	12.7	16.9	36.0	19.6	15.8	14.5	2.8	3.6	0.2	9.2	3.9	19.8	10.2
Carbonate	Dolomite	2.3	52.0	9.3	38.6	3.8	12.0	7.8	29.4	7.7	30.3	3.8	74.4	9.8	68.2	14.6	14.0	9.7
Carbonate	Calcite	0.4	3.5	2.8	1.7	0.9	17.7	1.7	12.7	4.5	7.8	1.3	1.8	10.2	3.7	7.1	1.3	
Feldspar	Albite		16.0		17.4		18.5		13.4	1.0	11.0	2.2	4.2	4.3	2.2		7.8	
Feldspar	K-Feldspar																	
Feldspar	Orthoclase						5.4							3.2		8.8		
Feldspar	Anorthoclase																	
Feldspar	Microcline							1.6		1.2			1.7		1.0			
Feldspar	Anorthite											6.3		0.5				
Amphibole	Hornblende		3.9				3.3											
Amphibole	Tremolite				4.1									3.7				
Mica	Muscovite								4.2					5.0		1.9	5.7	6.1
Mica	Biotite		1.7															
Mica	Phlogopite				6.2												12.5	
Silicate	Titanite					4.8												
Zeolite	Clinoptilolite								1.6								6.5	
Zeolite	Mordenite		0.4															
Pyroxene	Diopside						2.5											
Phyllosilicate	Talc																	
Silicate	Cordierite				1.4													